DEVELOPMENT OF A MICRO–FABRICATED COLLOID THRUSTER ARRAY

Luis Fernando Velásquez García
PhD candidate, Aeronautics and Astronautics, MIT

Manuel Martínez–Sánchez
Professor, Aeronautics and Astronautics, MIT

Akintunde I. Akinwande
Professor, Electrical Engineering and Computer Science, MIT

Abstract

The present paper describes the progress in the development of a micro–fabricated colloid thruster array able to produce thrust up to 80 mN and 1000 s. of I_{sp}. The paper addresses the concept, fabrication procedure and fabrication results of the engine and the latest fabrication version of the electrode system. In particular the issue of the spout design and formation is covered in some detail. The paper finally points out the near future goals of the project.

Introduction

Miniaturization of high-performance propulsion systems, particularly Electric Propulsion, has lagged behind the trend of the satellite field to undergone dramatic size and power reductions. This is in part due to unfavorable scaling laws for plasma-based thrusters of the types most commonly associated with kW-level operation.

Colloidal thrusters are electrostatic accelerators of charged droplets that are neutralized either by bi–polar operation mode of the engine (where droplets of opposite charges are extracted from different emitters while conserving overall neutrality) or by a downstream electron stream. The charged droplets are obtained from a conductive liquid meniscus when an electrostatic effect, named a Taylor cone[3], takes place if the liquid is influenced by a high enough electrostatic potential. A colloid emitter schematic can be seen in Figure 1

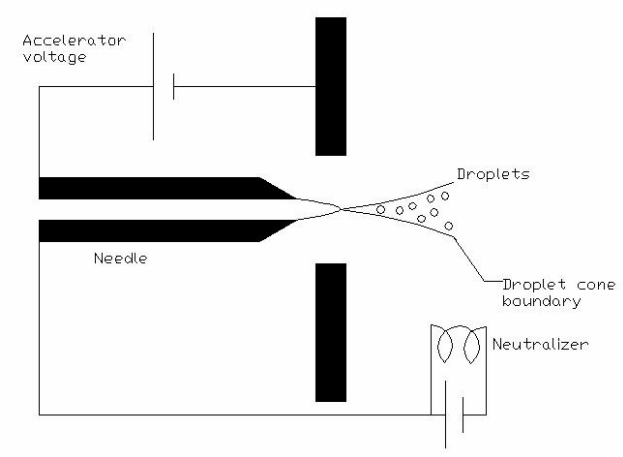

Figure 1. *Schematic of a basic colloid emitter.*

The technology of Colloid Thrusters, which first appeared some thirty years ago[1], [2], has been identified as one that escapes these limitations and can exploit micro-fabrication techniques. This is because, among other reasons, Colloid thrusters can provide deltas of thrust down to tens of nano-Newtons, and second, the charged particles are extracted directly from a liquid without the need for electron collisions, and so the plasma scaling limitations do not apply. These thrusters can operate, depending on design, at high efficiency and moderately high specific impulses, between 400 and 1500 s.

Colloid thrusters can potentially be designed to cover an enormous range of thrust and power, by batch production of emitters through micro-fabrication procedures. This range can extend from the nano-Newton range, as needed for high precision disturbance cancellation, to the milli-Newton range, of interest for prime propulsion.
Micro-fabrication technologies address the problem of building a colloid thruster composed of many colloidal emitters on a small surface, while keeping costs down. It addresses as well the issue of emitter–to–emitter uniformity within an engine and repeatability from one engine to another.
During the last three years the Space Propulsion Laboratory at MIT's Colloid Thruster Program has been developing a micro-fabricated colloid thruster array as part of its research goals in Colloid Thruster technology. The design contemplates building a colloidal engine array using weakly doped p–Si wafers as substrate with some novel micro-fabrication technology (mostly plasma processing) such as RIE, DRIE and contact photolithography, using special recipes, developed exclusively for the engine. The dimensions and tolerances of the colloid engine have been set to allow for a worst–case misalignment of up to fourteen microns, even though the masks have an aligning mark system with a precision of 1.2 μm or better. The design decouples the hydraulic and electrical parts of the engine, to be joined by a self-aligned clip-like structure that facilitates the fabrication procedure and enhances the electrical safety.

The engine concept
The micro-fabricated thruster that has been developed at MIT is a direct application of an engine design concept that allows building a colloid emitter array based on almost any working fluid while allowing electrical control of the whole engine operation –no decoupled pumping system or neutralizer-. This philosophy can be summarized as follows[4], [5], [6]:

- The stagnation pressure in the tanks of the colloid engine must be such as to push through the ducting hydraulic impedance a flow-rate that falls within the range that can be pumped stably by the Taylor cones while the electrodes are activated.
- The stagnation pressure in the tanks must be smaller than the maximum pressure that can be supported by the meniscus of the emitters. This ensures that no flow is possible unless the extractor electrodes are activated.
- In order to produce a flow and thus activate the engine, an electric potential is applied between the extractor electrode and the emitter. The difference between the maximum pressure supported by the meniscus and the stagnation pressure is electrically provided by the extractor electrode. The smaller this pressure difference, the lower the starting potential that has to be provided between the emitters and the extractor electrode. A lower limit to this potential is imposed by the need to sustain the strong normal fields at the tip during steady operation as will be seen later.
- For most electrolytes, flow rate matching implies a high ratio of length–to-characteristic cross section length. Given the state of the art of micro-fabrication technology, the best way to obtain this high L/D ratio for a cross-section that can be dimensionally controlled is by carving the flow channels along the top surface of the wafer.
- By using the engine body as ground electrode and applying both negative and positive potentials as extractor electrodes to different emitters, droplets with both charge signs are obtained, allowing a net charge balance in the engine. Therefore, the engine neutralizes itself. This removes the need to include a power–costly neutralizer as part of the total engine system.
- The engine has two electrodes systems: an extractor that applies just enough potential to produce the Taylor cones, and an accelerator to achieve the desired I_{sp}. If just one electrode system is used, the voltage required for acceleration might be high enough to generate more than one Taylor cone per emitter, which is not desired in this engine design.

Engine Description
There are two versions of the micro–fabricated colloid engine in current development at MIT: a 4" wafer version and a 6" wafers version. The 6" wafer version is more advanced, with a more robust micro–fabrication process and smoother hydraulics. Some of the development of the 4" wafer version appears in previous references[4], [5]. This article focuses on the most recent 6" wafer version. The 6" wafer engine is composed of a bottom wafer, where most of the hydraulic system is formed, and a top wafer that seals the hydraulics. The hydraulic system is composed of a liquid reservoir, a manifold system, an array of channels,

a set of spouts and a couple of electrodes[6]. The liquid reservoir has an inlet for receiving both, propellant from the engine exterior and the pressure required to make the engine work in the intended regimen. The manifold system distributes the liquid to the emitters via the array of channels that provide the hydraulic impedance the engine needs. The emitters are composed of the external openings of the channels and the spouts of the engine (intended to avoid wetting problems and to locally enhance the electric field so the engine can be started with a lower voltage). A schematic of both the bottom wafer and the upper wafer can be seen in Figure 2

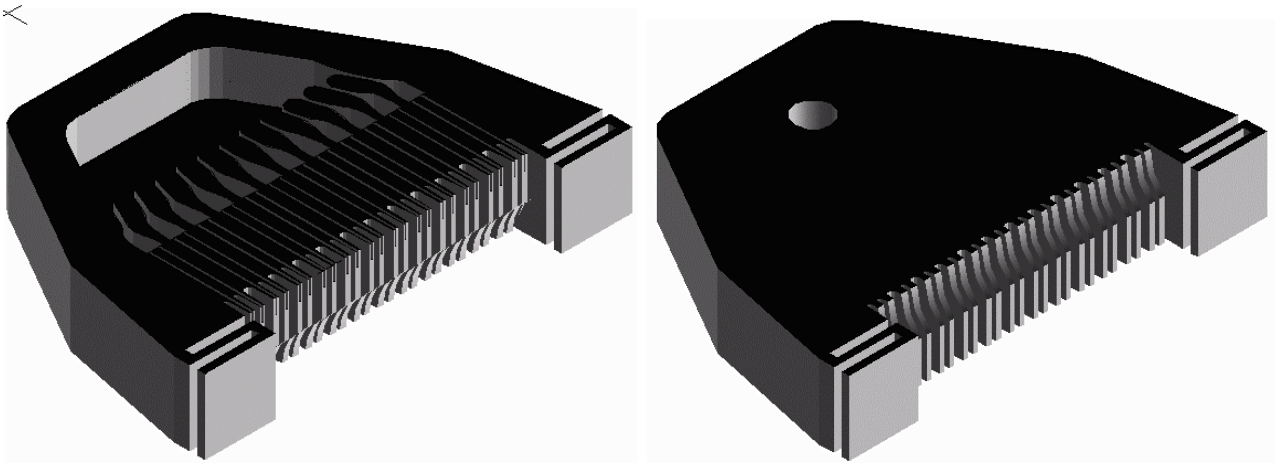

Figure 2. *Schematic of the bottom wafer of a 6" wafer colloid engine (left) and of the top wafer of a 6" wafer colloid engine (right) . In the bottom wafer the liquid reservoir, manifold system and array of channels can be seen as well as the lower portion of the spouts. In the upper wafer the propellant inlet and the upper portion of the spouts can be seen. The s–like structures on both sides of the array of spouts represents the clip system that eventually assembles the hydraulics with the electrical system. The thickness dimension is greatly exaggerated.*

A schematic of the hydraulic system of the engine can be seen on Figure 3. The hydraulic system is connected to the electrical system via a set of clips, spring–like structures intended to align both systems. Those structures have been designed to have a maximum stress level of 1GPa when in maximum deflection, including some possible failure modes for mishandling the assembly. Figure 4 shows a 3–D view of the clip concept while Figure 5 shows the displacement field and stress distribution computed for the clip structure when working properly.

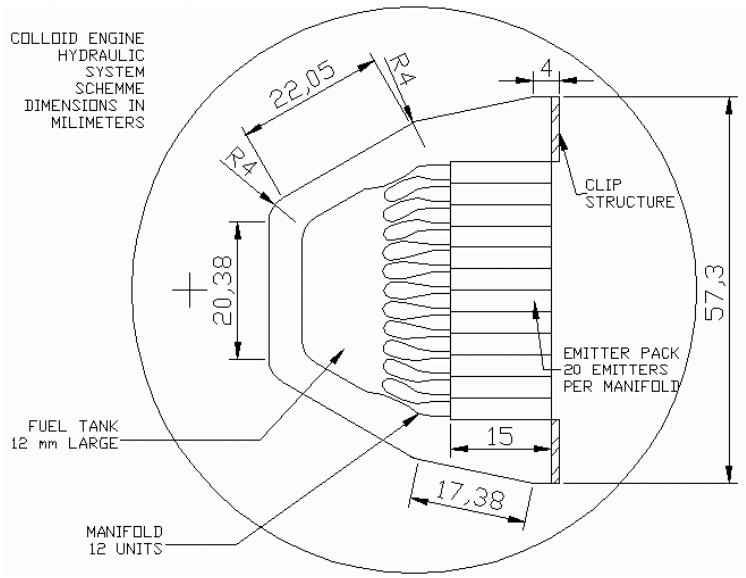

Figure 3. *Schematic of an MIT colloid engine in its 6" wafer version.*

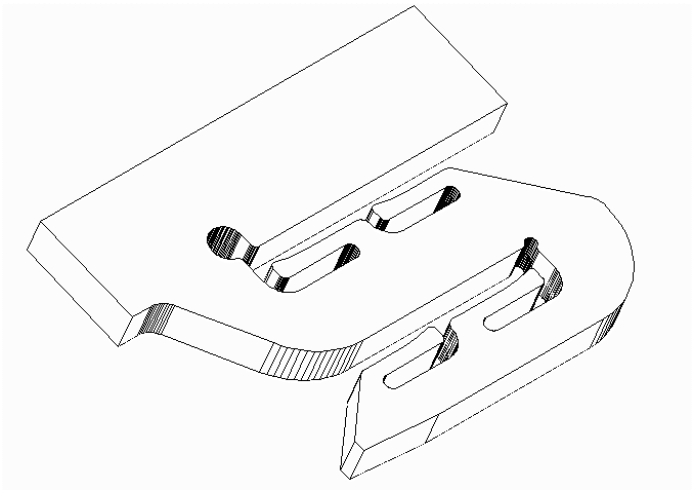

Figure 4. 3–D *Schematic (with its real proportions) of a clip set of the MIT colloid engine in its 6" wafer version. The spring gap is 420 μm, the effective spring length is 1400 μm and the spring constant is about 10000 N/m.*

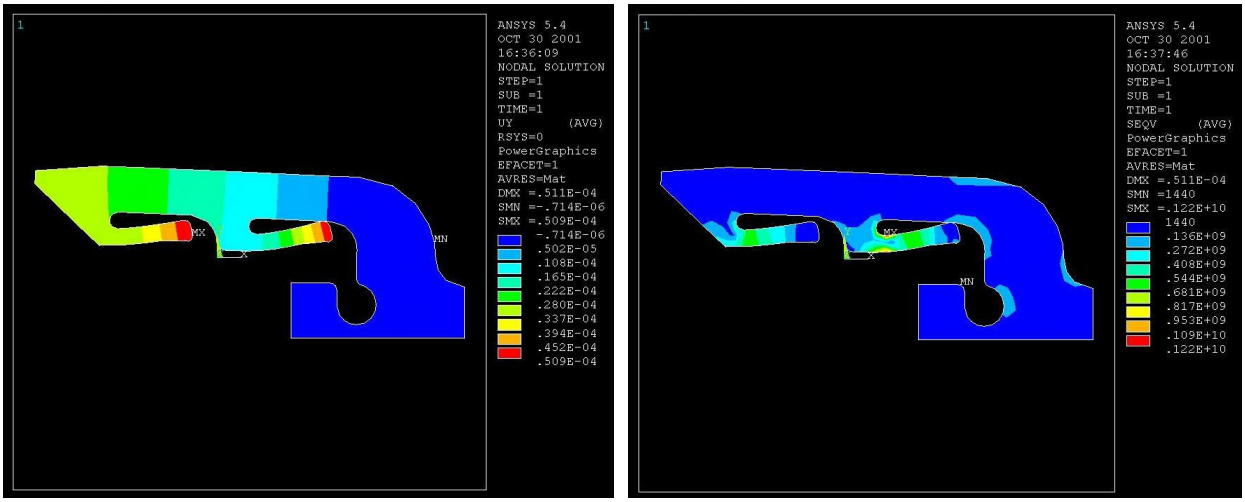

Figure 5. *Finite Element solution for the displacement (left) and maximum stress (right) of the clip structure for the case when the device is properly operated. The springs are intended to deflect 50 μm without exceeding 1 GPa of maximum stress.*

The clip design is currently in the process of undergoing tests to diagnose its limitations (one of the core questions not yet solved is if the smoothness of the DRIE –Deep Reactive Ion Etching– is good enough so it does not substantially affect the performance of the material when stressed).

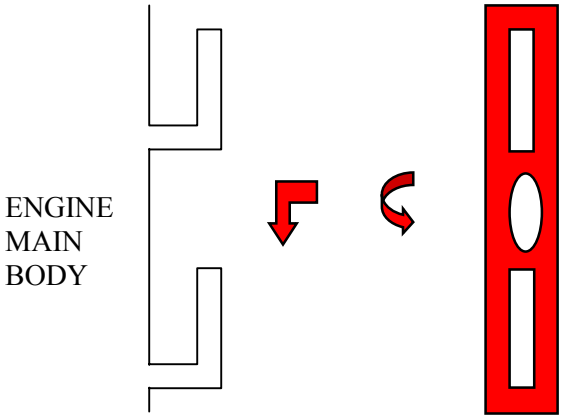

Figure 6. *Schematic of how the hydraulics and the electrodes are assembled.*

Figure 6 shows a schematic of how the hydraulics and the electrodes are assembled: the electrodes, as will be seen later, are produced from lightly doped p–Si wafers. These electrodes have a pair of slots on both ends to allow the clips to slide. The slots have as well a set of springs to control the assembly in two orthogonal directions. The idea is then to hand assemble the engine such that by sliding the clips into the slots, the electrodes align to the spouts.

Hydraulics Micro–fabrication process

The process starts with 350 μm thick lightly doped p–Si wafers. From each wafer couple six engines are obtained. To clarify the explanation the following figures show an analogous process where just one engine per wafer is formed and the inherent proportions between the different engine parts are altered so it is possible to appreciate the engine parts with one scale. For each step, core pictures of the actual procedure are shown, except in the final step, where the spouts are formed, because this step is discussed in more detail in a later part of this article.

The first step, after transferring on both sides of the wafer the set of features that will allow the builder to align the different masks and measure the features that have been created, is to carve across the top surface of the bottom wafer (the one that has most of the hydraulic system) the channels that are going to provide the hydraulic impedance. This etching is done with a novel recipe based on a Cl_2 plasma that has been tested to go as deep as 25 μm with an aspect ratio of 2V:1H. Figure 7 shows a schematic of a wafer after the channels are formed and Figure 8 shows SEM pictures of the channel cross–sections. The cross–section of the channels shows 90^o walls for two thirds of the depth and about 82^o for the portion closest to the bottom. In contrast, standard photoresist is usually no steeper than 64^o.

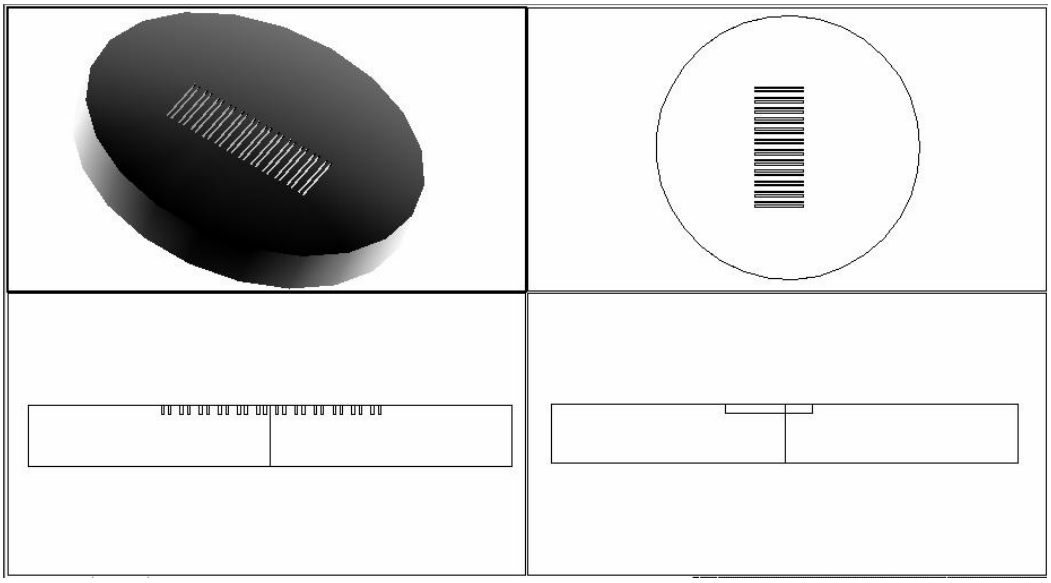

Figure 7. *Schematic with a 3–D isometric and principal views of a wafer after the channels are formed.*

After the channels are done, a nested mask approach is used to form both the liquid reservoir and the manifold system. This is a stratified etching because it is intended to provide the engine with as much stiffness as possible without sacrificing the amount of liquid the engine can carry internally. A pair of masks is used for this purpose and two films of silicon oxide and photoresist are used as etching masks. Each etching is about 60 μm deep due to the occurrence of major roughness when the etching is substantially deeper. This roughness is the saturation result of the nature of DRIE: a set of isotropic etchings followed by a passivation phase where polymer is deposited. In order to avoid stress concentrations from the actual fabrication procedure a SF_6 plasma–based etching was selected so that the liquid reservoir and the manifold system are carved with a mirror–like finish.

The engine has a set of columns across the reservoir surface to reduce the deflection of the upper and lower walls of the container due to the pressure difference across them. Figure 9 shows a schematic of a wafer after the reservoir and manifolds are formed while Figure 10 shows SEM pictures of the fabrication results during tuning.

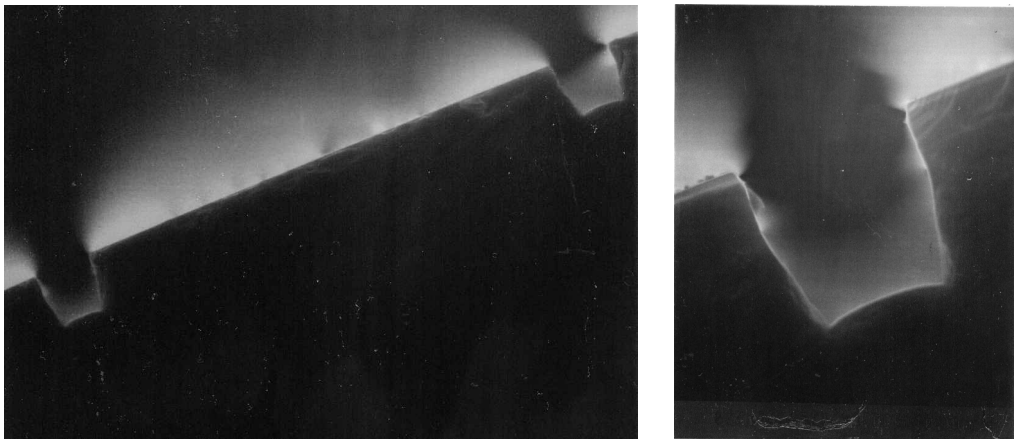

Figure 8. *SEM pictures of two adjacent channels separated 130 μm (left) and a zoom of the channel cross–section with vertical and horizontal dimensions of 12 μm (right). Notice the almost perpendicular walls of the channel. In the upper part of the cross section the silicon oxide film used as etching mask can be seen.*

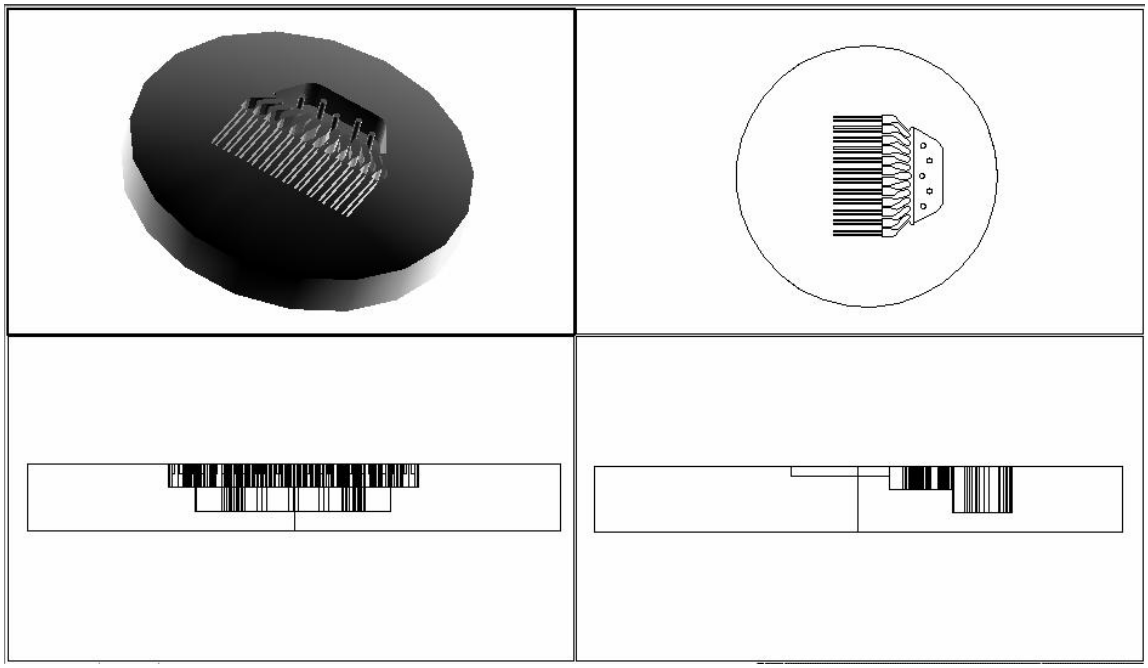

Figure 9. *Schematic with a 3–D isometric and principal views of a wafer after the liquid reservoir and the manifold system are formed.*

After the hydraulic system is formed, a thin layer of oxide is thermally grown on both wafers (the wafer that has the hydraulics and the wafer that is intended to seal the hydraulic circuit). The purpose of this film is to provide a practical way to localize the center of the wafer system when etching the spouts. After the oxide is formed the two wafers are fusion–bonded. Figure 11 shows a schematic of the fusion bonding operation and some infrared pictures of the bonding process.

Except for the electrode formation, which is done in a different substrate, what remains to be done is the engine extraction (done with DRIE) and the spout generation. A subsequent mask forms the lower lip of the spouts (this step is done with an SF_6 based plasma) while a nested mask approach forms both the upper lip of the spouts and the engine endings (the upper lip is formed by an isotropic plasma as well while the engine endings are done with DRIE). In this final step the clips are formed as well. Figure 13 shows a schematic of the formation of the lower lip of the spouts while Figure 14 shows a schematic of the upper lip formation. A view of the final result is shown in Figure 2.

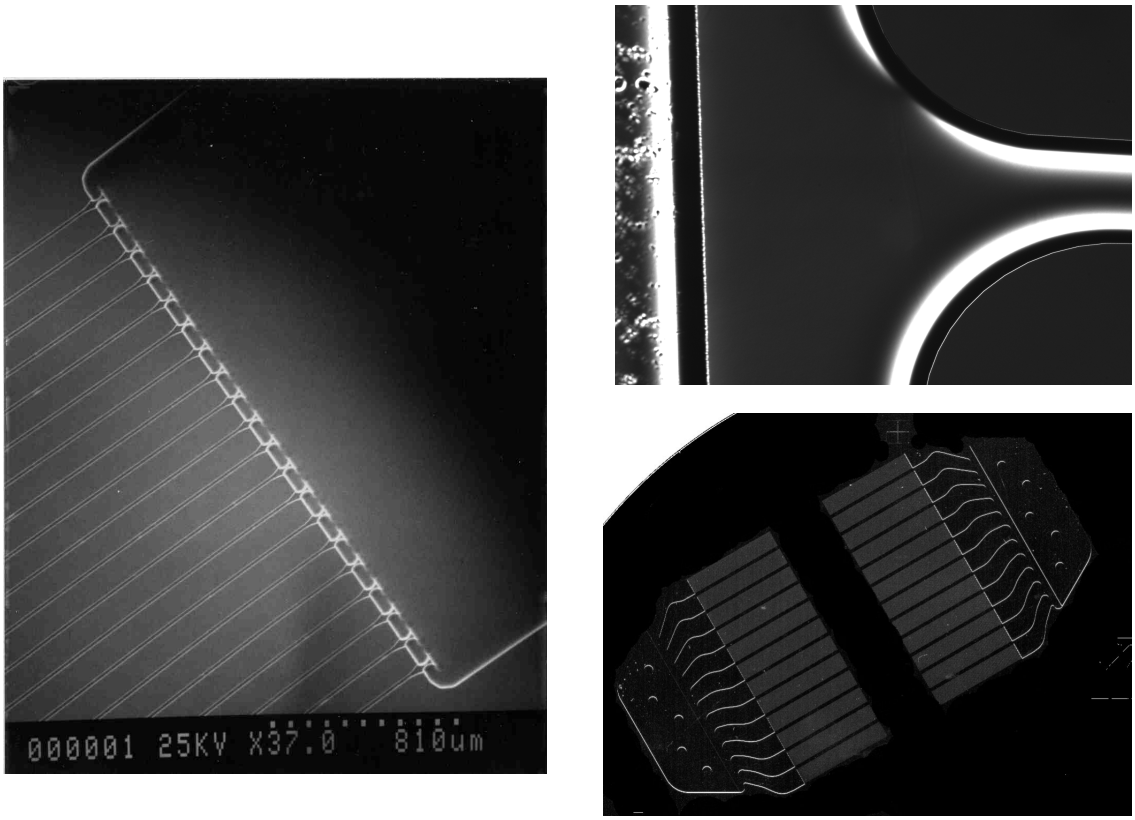

Figure 10. *SEM pictures of the part where a manifold evolves into a set of channels (left), the notching problems on the bottom wall of the liquid reservoir when deepened too much (upper right) and a zoom of two adjacent hydraulic systems (lower right). Notice the set of columns to reduce the wall deflection in the liquid reservoirs and the smoothness of the etching due to the isotropic plasma recipe.*

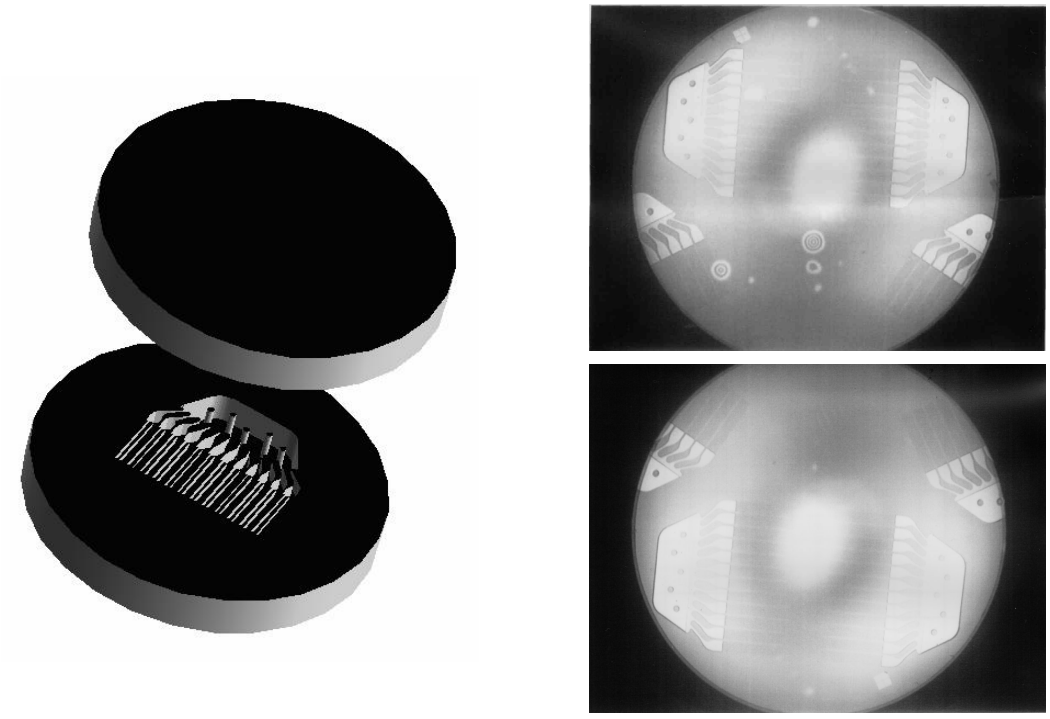

Figure 11. *Schematic with a 3–D isometric of the wafer bonding process (left) and infrared pictures of a pair of wafers after Van der Waals bonding (upper right) and after 1050 º C annealing in a nitrogen atmosphere (lower right). The wafer system later grows 1.5 microns of oxide for later use in the engine ending formation and the spout formation. Notice the presence of Newton rings in the wafer interface when just bonded by Van der Waals forces and how those defects are not visible after annealing.*

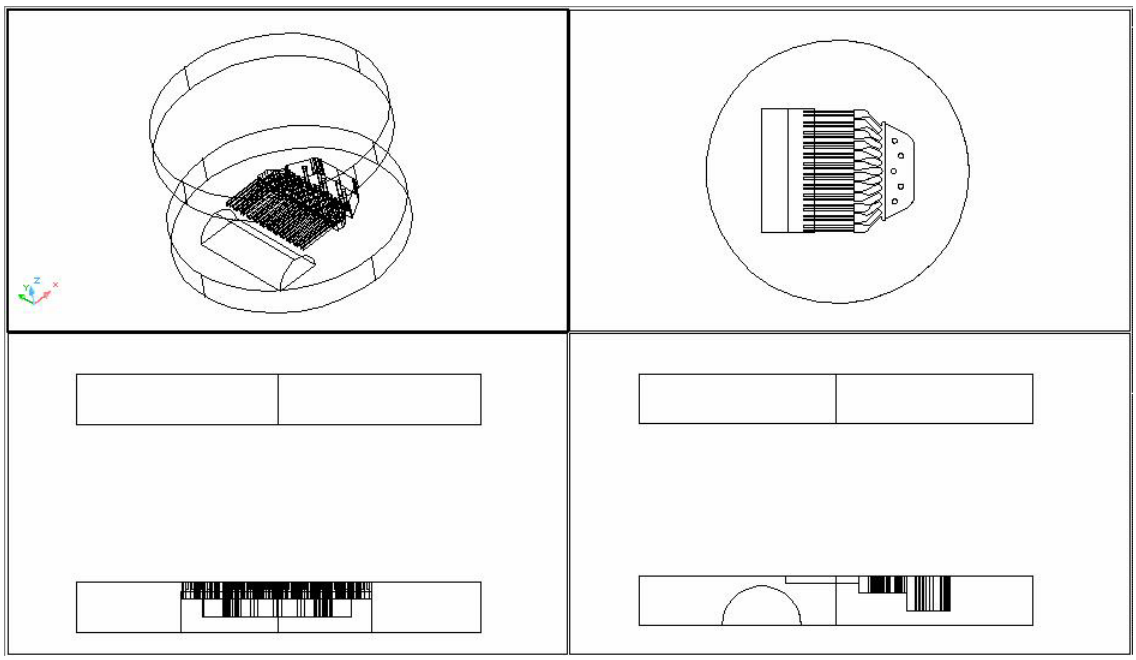

Figure 12. *Schematic with a 3–D isometric and principal views of the lower lip formation.*

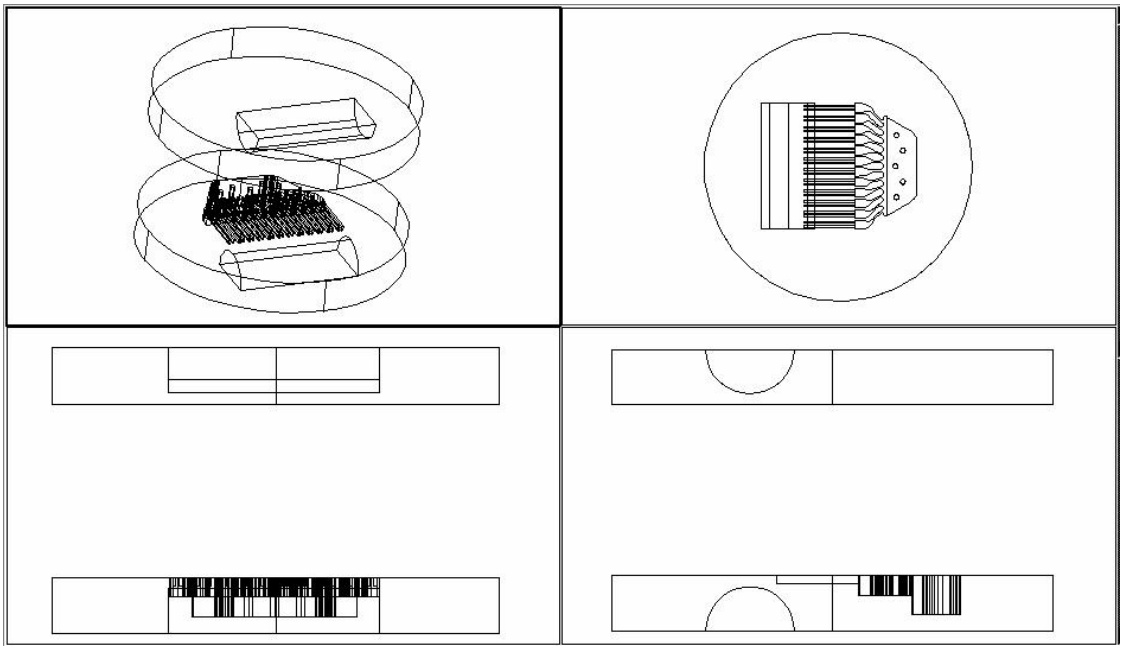

Figure 13. *Schematic with a 3–D isometric and principal views of the upper lip formation. The two wafers are shown separated for a better understanding of the process step.*

Electrode system fabrication process

The fabrication of the electrode system is in its initial stages: the optical masks are being made and we expect to start the fabrication by the time of the presentation of this article in the International Conference. The process starts with lightly doped p–Si wafers 365 μm thick. After patterning the cross hairs and the set of features to help diagnose the fabrication progress, 1 micron of CMOS grade thermal oxide is grown and after that 9 microns of silicon oxide are deposited on both sides of the substrate with PECVD –Plasma Enhanced Chemical Vapor Deposition–. The film is then annealed in an atmosphere of nitrogen and oxygen to both reduce stresses and fill in possible film gaps due to hydrogen trapped when the PECVD was performed. After the electrical insulation is formed, a thin film of poly–Si is deposited with LPCVD on both sides of the wafer to form the etching masks later to be used for patterning: first a poly–Si etching mask is patterned so

that the clip slots, engine endings and the gap to allow the charged droplets pass through the electrode can be later etched, as shown in Figure 14; then the other poly–Si side is patterned as etching mask for later removing substrate material that could otherwise be hit by the droplets, as shown in Figure 15.

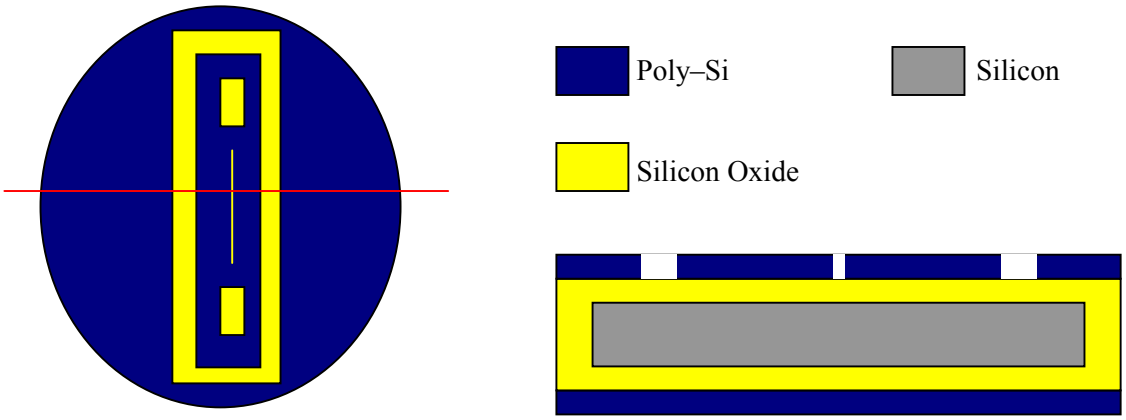

Figure 14. *Schematic of the top view and cross–section of a wafer after the poly–Si is deposited and the upper side is patterned.*

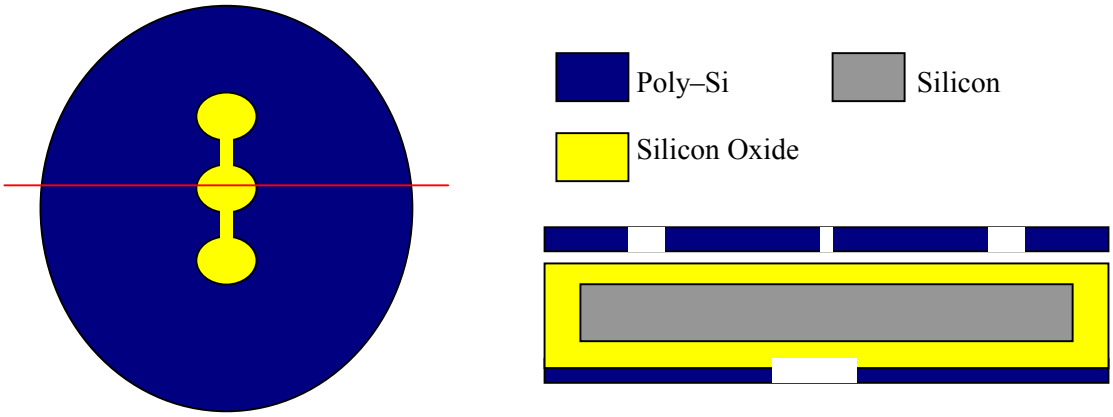

Figure 15. *Schematic of the bottom view and cross–section of a wafer after the poly–Si is deposited and both the upper and lower sides are patterned. Notice that the lower cut forms a set of ribs to stiffen the electrode in the region of the droplet gap, while removing most of the material that can be sputtered by the droplets.*

After patterning the poly–Si film, its features are transferred to the silicon oxide by using a organic–based plasma. The Poly–Si film is then removed with an SF_6 based plasma. The silicon oxide film is patterned because it is going to be used as etching mask as well in the DRIE steps, including the isotropic versions of them, due to its high etching selectivity compared to silicon.

After the etching masks are transferred to the silicon oxide film, PVD –Physical Vapor Deposition– titanium and PVD tungsten are deposited as field films. The titanium film provides a better adhesion of the tungsten film to the substrate while the tungsten film is intended for protecting the film integrity from the sputtering caused by the charged droplets. If the titanium film is not covered with the layer of tungsten it will probably oxidize up to a point where its electrical conductivity will substantially diminish.

The electrode paths are then patterned with a novel plasma chemistry. The electrode is connected to the external circuit by means of a pad that is in physical contact to the electrode paths. The pad is formed at the same as the electrode paths are etched (a welding point is put there as interface between the external circuitry and the electrode). What remains to be done is etching the features transferred to the silicon oxide film, that is to etch the clip slots, the gap for the droplets and the thinning of the substrate so the droplets do not hit the electrode body. A schematic of the final result is shown in Figure 16.

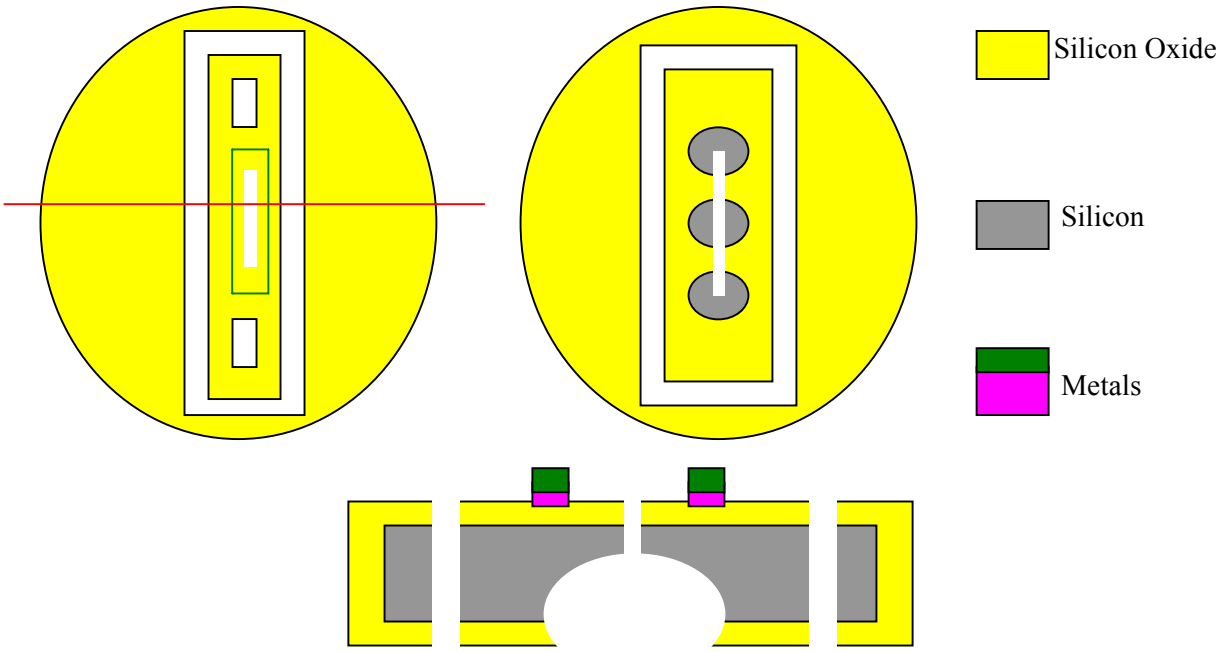

Figure 16. *Schematic of the top view (upper left) bottom view (upper right) and cross–section (bottom) of a wafer after the complete electrode fabrication process is carried out. Notice the electrode surrounding the gap that will face the spouts.*

The spout generation

The formation of the spouts might be the toughest part of the engine production and its quality heavily impacts the engine performance. It involves two of the last three masks and is difficult because:

- It is proposed to use a nested mask approach with a isotropic–anisotropic regimen.
- Because of this most of the time the etching mask that defines de geometry of the spouts is in cantilever with a large free dimension. The etching mask that eventually shapes the spouts acts as an umbrella, being forced by ion flux towards the substrate.
- The etching involves three plasma etching steps: they should be done one after another to minimize the risk of the etching mask falling off.
- Depending on how sharp the spout lips are created, the threshold voltage to turn on the engine is substantially influenced.

The starting voltage and electric field in the emitter tip are known to be approximately given by[7]

$$V_{START} \cong \sqrt{\frac{\gamma L_c}{\varepsilon_o}} \cdot \ln\left(\frac{4d}{L_c}\right) \qquad E_{START} \cong 2\sqrt{\frac{\gamma}{\varepsilon_o L_c}} \qquad (1)$$

where γ is the liquid surface tension, Lc is the characteristic length of the spout, d is the distance between the spout and the electrode, and ε_o is the electrical permitivity of free space. It is clear that a smaller characteristic length of the spout will reduce the starting voltage and that to first order the dependence of the starting voltage on the spout–electrode separation is logarithmic. 2–D, 2–D axis–symmetric and 3–D Finite Element Analyses of the external electric field have been carried out. For the 3–D cases we analyzed both a smooth spout system with large spout–to–spout separation (so the spouts do not interfere between each other) and the real spout system with its spout–to–spout separation of 130 μm. For the case of the real spout system, three electrode separations where used: 50 μm, 140 μm and 500 μm. For the other cases the default electrode – to spout separation was 50 μm. With the default electrode–to–spout separation those simulations predict that the maximum electric field on the spout surface is about the applied voltage divided by two times the characteristic length. The characteristic length is assumed to be the diameter in the case of a circular–like cross section of the tip spout, or the side of the square in a square–like cross section for the spout locally in its tip. Based on equation (1), we expect to need about 4×10^7 V/m to produce the Taylor cones on the

meniscus of the spouts, and this field would be generated by about 1100 V applied between the extractor electrode and the spouts if the real spout system and the default electrode–to–spout separation are used. The electric potential used in all the simulations was 1000 V. The electric field value that is important from the simulations is the value of the mean field that surrounds the spout, which as rule of the thumb is about three quarters of the maximum electric field on each simulation. The following conclusions can be extracted from the simulations:

- There is a strong difference between the 2–D model and the axi–symmetric model. With the same characteristic length and electrode–to–spout separation the axi–symmetric model predicts an electric field twice as large as the maximum electric field of the 2–D simulation.
- The 3–D case where the spouts have the same characteristic length but are spaced 500 μm (enough distance to avoid interference between them) shows an electrostatic solution practically identical to the axi–symmetric case.
- Our real spout system is closer to the 2 –D case than to the axi–symmetric case. We believe the spout–to–spout spacing is not large enough to fully take advantage of the 3–D nature of the spouts. This fact influences the minimum starting voltage but the geometry is good enough to concentrate most of the potential drop around the spouts, within a characteristic length from their tips.

Contrary to the suggestion from the approximate equation (1), there is some distance dependence on the maximum electric field with respect to the electrode–to–spout separation. The closer the electrode is to the meniscus, the less voltage is needed to reach the threshold condition. Figures 17, 18 and 19 show some of the FEA results obtained with the software package Maxwell. We hope the spouts will work with less potential than predicted because they have sharp internal corners and the exit of the channels have on the bottom of the cross section a trenching adjacent to the vertical walls (see Figure 8) that should locally enhance the electric field. We know experimentally that a capillary with a square cross section needs about 20% less starting voltage than a circular one of same characteristic length, presumably due to the enhancing effect of the sharp corners of the square.

Substantial advance has been achieved on the fabrication of the spouts, but we have been slowed down by the need to trade off between robustness and performance. Figure 20 shows the production of the spout system without its 3–D electric field enhancing capabilities and the concept of a nested mask approach with isotropic–anisotropic plasma regimens is also demonstrated; Figure 21 shows a series of SEM of the production of the upper lip and the spout–to–spout separation, the two more difficult of the three steps for building the spout system.
A test of the fabrication of the whole spout system is under execution, and pictures of it including the lower lip might be available by the time of the conference.

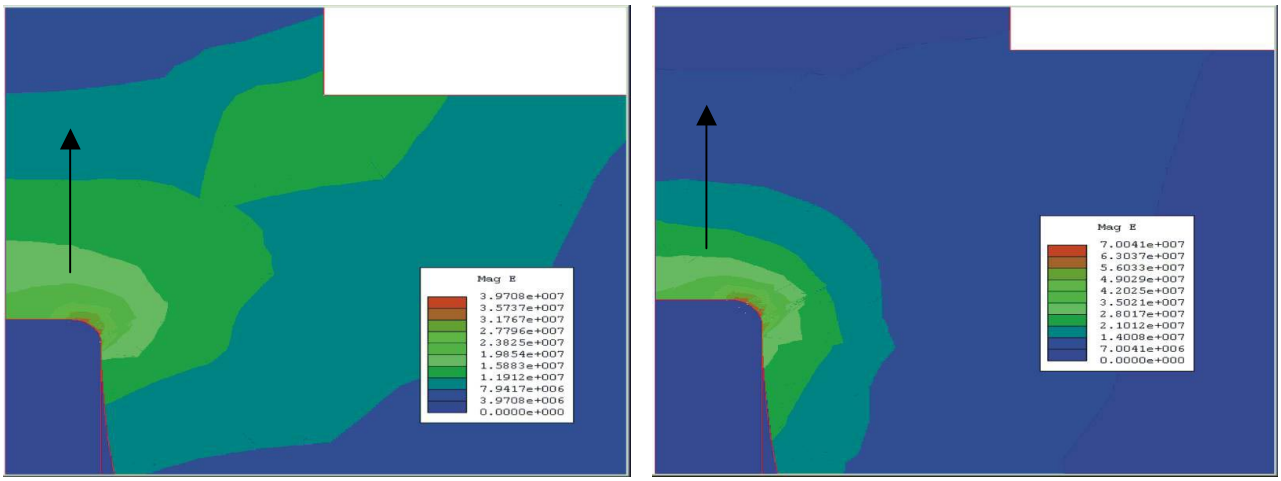

Figure 17. *The electric field outside the spouts. 2–D simulation, electrode–spout separation of 50 μm (left); 2–D axis–symmetric simulation, electrode–spout separation of 50 μm (right). The axis–symmetric solutions gives almost twice the electric field compared to the 2–D solution. The black arrows show the direction of movement of the droplets that leave the emitter. The white space on the upper right corner is the extractor electrode. The blue body inside the colored field is the tip of the emitter.*

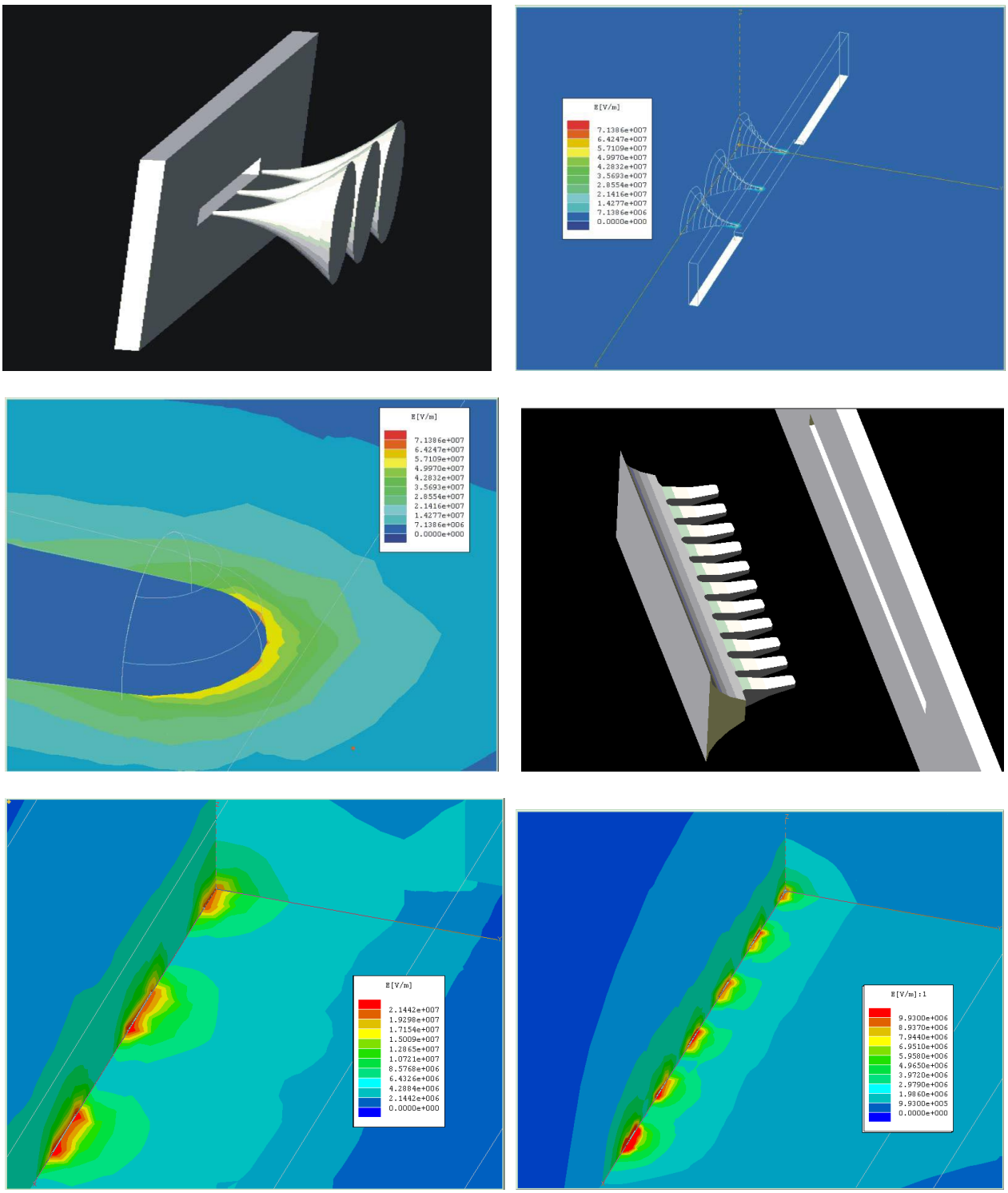

Figure 18. *The electric field outside the spouts. 3–D view of the smooth spout system with large spout–to–spout separation (upper row, left); 3–D simulation, smooth spout system with large spout–to–spout separation, electrode–spout separation of 50 μm (upper row, right); zoom in the central emitter of the 3–D simulation, smooth spout system with large spout–to–spout separation, electrode–spout separation of 50 μm (middle row, left); 3–D view of the real spout system (middle row, right) –the spout–to–electrode separation is exaggerated to clarify the set up–; 3–D simulation of the real spout system, electrode–spout separation of 140 μm (lower row, left); 3–D simulation of the real spout system, electrode–spout separation of 500 μm (lower row, right).*

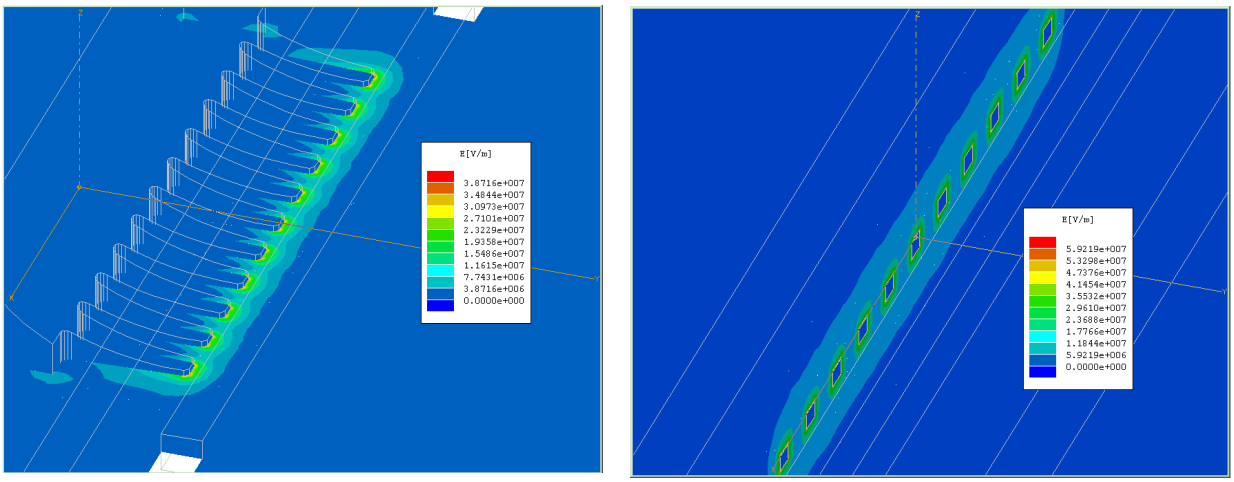

Figure 19. T*he electric field outside the spouts3–D simulation of the real spout system, electrode–spout separation of 50 μm (left and right).There is a substantial difference between these two pictures, possibly due to the occurrence of sharp corner effects in the solution read by the sampling plane used for the picture on the right.*

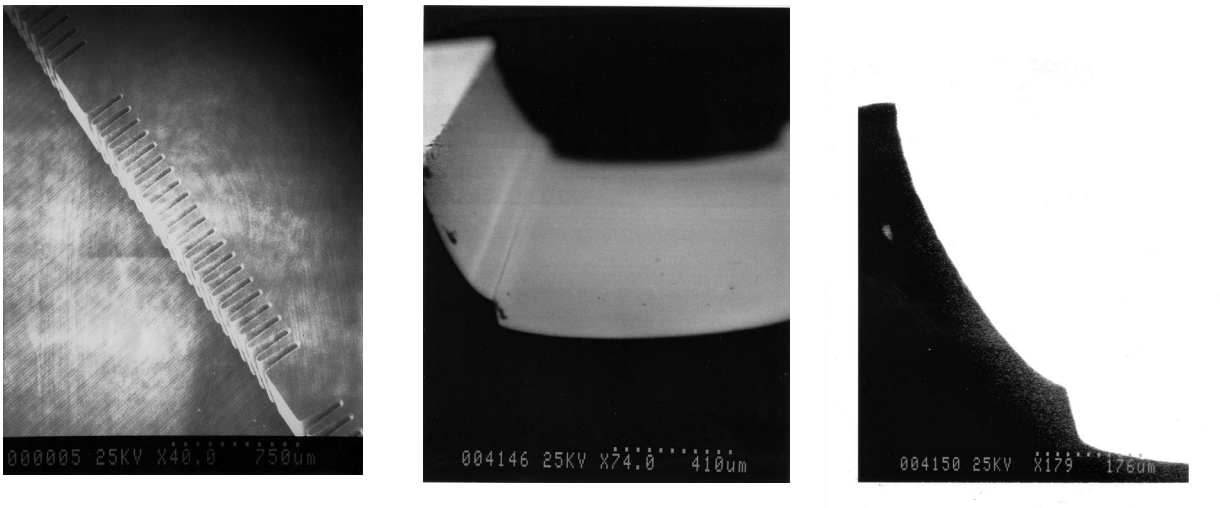

Figure 20. *SEM pictures of an engine with the spout system formed, without the enhancing capabilities that the lips would provide (left), and the testing of the nested mask approach with isotropic–anisotropic plasma regimens (center, right). The lips, formed by the isotropic part of the nested mask procedure, are intended for enhancing locally the electric field and avoiding wetting problems as well.*

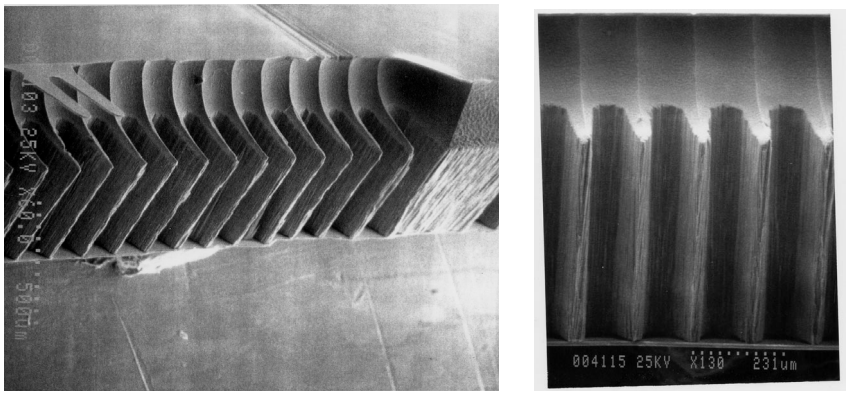

Figure 22. *SEM pictures of the upper lip and the spout–to–spout separations formed. The etching mask, made of silicon oxide, is visible in the aerial view of the set of spouts (left). There is as well a front view of the spouts, showing the straightness of the etching, even though is was controlled by an umbrella–like etching mask. The film that can be seen on the bottom is silicon oxide, intended for producing the lower lip of the spouts.*

Future Work

After building the engine some tests should be done in order to verify its performance:

- Testing of the wafer–to–wafer sealing. This also includes maximum chamber pressure before structural breakdown and it is strongly related to the overall smoothness of the fabrication process.
- Taylor Cone stability, continuity.
- Visually diagnosing the percentage of emitters that are working.
- Minimum turn–on voltage.
- Thrust, current carried by the jets, operational flow-rates, characterization of the hydraulic impedance of the engine.

In order to perform all this testing a suitable facility is under assembly and it is expected to be finished by the time the first set of engines is ready for trying.

Aknowledgement

This work is made possible by the support from the AFOSR, Grant F49620-01-1-0398, Mitat Birkan technical monitor.

References

[1] Cohen, E., "A 100 kV 10 w Heavy Particle Thruster, Paper AIAA 65–377, AIAA Second Annual Meeting, S. Francisco, CA, 1965.

[2] Daley, H., "Colloid Annular Array Thruster Development", AIAA 10th Electric Propulsion Conference, Lake Tahoe, Nevada, 1973.

[3] Taylor, G. I., "Disintegration of Water Drops in an Electric Field", Proc. R. Soc. London A280, pp 383–397, 1964.

[4] Velásquez, L. F., "A Micro–Fabricated Colloid Thruster Array", MS Thesis, Massachusetts Institute of Technology, June 2001.

[5] Velasquez, L. F. "Micro–Fabrication of a Colloid thruster Array", 6th International Symposium Propulsion for Space Transportation of the XXIst Century, 14 – 17 May 2002, Versailles, France.

[6] Velasquez L. F., " A Micro-fabricated Colloid Thruster Array", AIAA–2002–3810, 38th AIAA/ASME/SAE/ASEE Joint Propulsion Conference & Exhibit, Indianapolis, Indiana 7–10 July 2002.

[7] Martínez–Sánchez, M., Space Propulsion Class Notes , Massachusetts Institute of Technology, 2001.